ResearchGate

See discussions, stats, and author profiles for this publication at: https://www.researchgate.net/publication/273066772

Is His54 a gating residue for the ferritin ferroxidase site?

ARTICLE *in* BIOCHIMICA ET BIOPHYSICA ACTA (BBA) - PROTEINS & PROTEOMICS · FEBRUARY 2015

Impact Factor: 2.75 · DOI: 10.1016/j.bbapap.2015.02.011 · Source: PubMed

CITATIONS
3

READS
49

4 AUTHORS:

Caterina Bernacchioni
University of Florence
21 PUBLICATIONS **341** CITATIONS
SEE PROFILE

Silvia Ciambellotti
University of Florence
4 PUBLICATIONS **4** CITATIONS
SEE PROFILE

Elizabeth C Theil
North Carolina State Univ., Raleigh, NC; & C…
209 PUBLICATIONS **8,209** CITATIONS
SEE PROFILE

Paola Turano
University of Florence
115 PUBLICATIONS **3,461** CITATIONS
SEE PROFILE

All in-text references underlined in blue are linked to publications on ResearchGate, letting you access and read them immediately.

Available from: Caterina Bernacchioni
Retrieved on: 24 January 2016

Biochimica et Biophysica Acta xxx (2015) xxx–xxx

Contents lists available at ScienceDirect

Biochimica et Biophysica Acta

journal homepage: www.elsevier.com/locate/bbapap

Is His54 a gating residue for the ferritin ferroxidase site?☆

Caterina Bernacchioni [a,b], Silvia Ciambellotti [a,b], Elizabeth C. Theil [c,d], Paola Turano [a,b,*]

[a] Magnetic Resonance Center CERM, University of Florence, Via Luigi Sacconi 6, 50019, Sesto Fiorentino, Florence, Italy
[b] Department of Chemistry, University of Florence, Via della Lastruccia 3, 50019, Sesto Fiorentino, Florence, Italy
[c] Children's Hospital Oakland Research Institute, 5700 Martin Luther King, Jr. Way, Oakland, CA 94609, USA
[d] Department of Molecular and Structural Biochemistry, North Carolina State University, Raleigh, NC 29695-7622, USA

ARTICLE INFO

Article history:
Received 3 November 2014
Received in revised form 17 February 2015
Accepted 18 February 2015
Available online xxxx

Keywords:
Ferritin
Ferroxidase site
Reaction kinetics
Mutagenesis

ABSTRACT

Ferritin is a ubiquitous iron concentrating nanocage protein that functions through the enzymatic oxidation of ferrous iron and the reversible synthesis of a caged ferric-oxo biomineral. Among vertebrate ferritins, the bullfrog M homopolymer ferritin is a frequent model for analyzing the role of specific amino acids in the enzymatic reaction and translocation of iron species within the protein cage. X-ray crystal structures of ferritin in the presence of metal ions have revealed His54 binding to iron(II) and other divalent cations, with its imidazole ring proposed as "gate" that influences iron movement to/from the active site. To investigate its role, His54 was mutated to Ala. The H54A ferritin variant was expressed and its reactivity studied via UV–vis stopped-flow kinetics. The H54A variant exhibited a 20% increase in the initial reaction rate of formation of ferric products with 2 or 4 Fe^{2+}/subunit and higher than 200% with 20 Fe^{2+}/subunit. The possible meaning of the increased efficiency of the ferritin reaction induced by this mutation is proposed taking advantage of the comparative sequence analysis of other ferritins. The data here reported are consistent with a role for His54 as a metal ion trap that maintains the correct levels of access of iron to the active site. This article is part of a Special Issue entitled: Cofactor-dependent proteins: evolution, chemical diversity and bio-applications.

© 2015 Elsevier B.V. All rights reserved.

1. Introduction

Maxiferritins (hereafter simply called ferritins) are iron storage proteins characterized by a highly symmetric overall structure, conserved in eukaryotes and prokaryotes [1–3]. The ferritin nanocage self-assembles from twenty-four 4-helix bundle subunits to provide an almost spherical protein shell with 432 point symmetry (Fig. 1A). Each ferritin subunit is enzymatically active (H-type) except in animal ferritins, which coproduce a catalytically inactive subunit (L type) that co-assembles with active subunits in H:L ratios that are tissue specific [4,5]. Amphibians have a further catalytically active type of subunits, called M (or H′). Homopolymeric animal ferritins composed by M or H subunits have been extensively studied as model systems for the iron biomineralization reaction [6,7]:

$$2Fe^{2+} + O_2 \rightarrow \left[Fe^{3+}\text{-}O\text{-}O\text{-}Fe^{3+}\right]$$
$$\left[Fe^{3+}\text{-}O\text{-}O\text{-}Fe^{3+}\right] + H_2O \rightarrow H_2O_2 + \left[Fe^{3+}\text{-}O\text{-}Fe^{3+}\right]$$
$$\left[Fe^{3+}\text{-}O\text{-}Fe^{3+}\right] + (H_2O)_{x+2} \rightarrow Fe_2O_3(H_2O)_x + 4H^+$$
$$2Fe^{2+} + O_2 + (H_2O)_{x+3} \rightarrow Fe_2O_3(H_2O)_x + 4H^+ + H_2O_2.$$

The first two steps of the reactions occur at the catalytic site (named ferroxidase or oxidoreductase site), hosted within the central part of the 4-helix bundle of the active subunits.

The exact definition of the residues binding iron during the catalytic reaction has been hampered for several years by the transient nature of the ferric species that form at the ferroxidase centers. The analysis of the available X-ray structures of animal ferritins with non-native divalent cations (Cu^{2+}, Co^{2+}, Zn^{2+}, Mg^{2+}) has revealed the presence of several amino acid side chains that can potentially act as metal ion ligands [8–10]; their number is larger than what needed to bind the pre-oxidation diferrous species and the diferric-peroxo (DFP, hereafter) and ferric-oxo/hydroxo products. The several potential metal binding amino acids in the same area have been proposed to play a role in regulating the access of the iron substrate to the reaction center [8–11].

The amino acid ligands of the dinuclear ferric-oxo/hydroxo species formed by the catalytic reaction have been identified in bullfrog M ferritin crystal structures at 2.7 Å resolution (Fig. 1B); they are Glu58, which bridges the two iron ions Fe1 and Fe2, monodentate Glu23 and His61 as Fe1 ligands and bidentate Glu103 as Fe2 ligand [8]. His54 was initially proposed as a possible ligand for ferrous ion entering the Fe2 site [8]. Recently, the ligands of the pre-oxidation diferrous species have been found to be the same as for the ferric form (PDB: 4MY7 and 4LQV) [12].

The same structures have revealed additional metal ions interacting with side chains other than those in the ferroxidase center, including

☆ This article is part of a Special Issue entitled: Cofactor-dependent proteins: evolution, chemical diversity and bio-applications.

* Corresponding author at: Magnetic Resonance Center CERM, University of Florence, Via Luigi Sacconi 6, 50019 Sesto Fiorentino, Florence, Italy. Tel.: +39 055 4574266.
E-mail address: turano@cerm.unifi.it (P. Turano).

http://dx.doi.org/10.1016/j.bbapap.2015.02.011
1570-9639/© 2015 Elsevier B.V. All rights reserved.

Please cite this article as: C. Bernacchioni, et al., Is His54 a gating residue for the ferritin ferroxidase site?, Biochim. Biophys. Acta (2015), http://dx.doi.org/10.1016/j.bbapap.2015.02.011

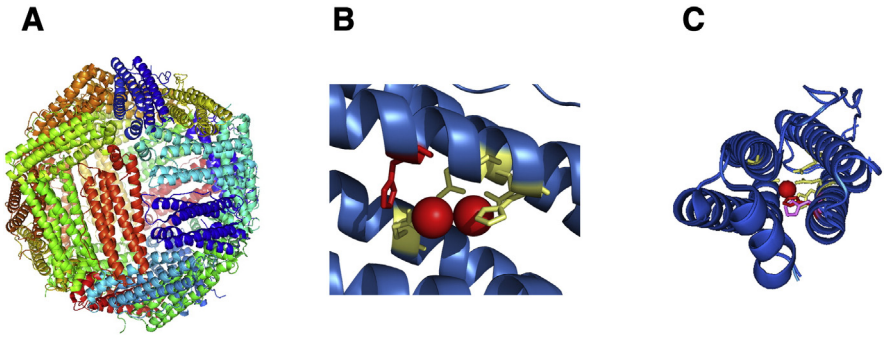

Fig. 1. The nanocage structure of bullfrog ferritin assembled from M subunits. Cartoon representation of the nanocage structure (A). Front (B) and side (C) close-up views of the ferritin monomer with the residues in the enzymatic ferroxidase site shown as yellow sticks. The swinging of the His54 ring from the distal (pink) to the proximal (red) conformation upon iron (red sphere) binding is highlighted in panel C. Drawn using PyMOL (PDB: 3RBC and 3RGD).

His54, that is differently populated at different times of free diffusion of iron(II) through ferritin crystals (PDB: 4LPJ, 4LQJ, 4LYX, 4LYU, 4LQV, 4LQN, 3RGD) [8,12].

The imidazole ring of His54 faces the inner cavity of ferritin and upon binding metal ions swings between two main conformations, named distal and proximal (Fig. 1C). This movement could be important to capture iron from the inner cavity and drag it inside the 4-helix bundle channel. On the other hand, it could also constitute an exit strategy for the ferric products migrating into the inner cavity.

Additionally, His54 has been observed to stably bind other transition metal cations such as Co(II) and Cu(II), [8,9], trapping them out from the metal binding site.

Here we have produced the H54A variant of M ferritin to remove any possibility of binding metal ions at this position and evaluated the effect of this substitution on the ferritin activity.

2. Materials and methods

2.1. Mutagenesis

Site directed amino acid substitution in bullfrog-M ferritin protein cages was generated by PCR, with expression plasmid pET-3a bullfrog-M ferritin DNA as template, using the QuikChange II site-directed mutagenesis kit (Stratagene). The DNA in the coding regions in all the protein expression vectors was analyzed for sequence confirmation (Primm srl, Milan, Italy).

2.2. Protein expression

pET-3a constructs encoding WT and H54A ferritins from the American bullfrog were transformed into *Escherichia coli* BL21(DE3) pLysS cells which were subsequently cultured in LB medium containing ampicillin (0.1 mg/ml) and chloramphenicol (34 μg/ml). Cells were grown at 37 °C, until $A_{600\ nm}$ reached 0.6–0.8 and subsequently induced with isopropyl 1-thio-β-D-galactopyranoside (IPTG, 1 mM final concentration) for 4 h. Recombinant ferritins were purified from the harvested cells, as described previously [13,14]. Briefly, cells were sonicated and the cell free extract obtained after centrifugation (40 min, 40,000 rpm, 4 °C) was incubated for 15 min at 65 °C as the first purification step. After removal of the aggregated proteins (15 min, 40,000 rpm, 4 °C), the supernatant solution was dialyzed against Tris–HCl 20 mM pH 7.5; applied to a Q-Sepharose column in the same buffer and eluted with a linear NaCl gradient of 0–1 M in Tris 20 mM, pH 7.5. Fractions containing ferritin, identified by Coomassie staining of SDS-PAGE gels, were combined and further purified by size exclusion chromatography using a Superdex 200 HiLoad 16/60 column.

2.3. Stopped-flow kinetics

Addition of 2 Fe^{2+} ions per subunit [15] or 4 Fe^{2+} ions per subunit in frog M ferritin, WT or H54A, was monitored as the change in $A_{650\ nm}$ (diferric peroxo; DFP) or $A_{350\ nm}$ ($(Fe^{3+}O)_x$) after rapid mixing (less than 10 ms) of equal volumes of 100 μM protein subunits (4.16 μM protein cages) in 200 mM 3-(N-morpholino)propanesulfonic acid (MOPS), 200 mM NaCl, pH 7.0, with freshly prepared solutions of 200 μM ferrous sulfate or 400 μM ferrous sulfate in 1 mM HCl in a UV/visible stopped-flow spectrophotometer (SX.18MV stopped-flow reaction analyzer, Applied Photophysics, Leatherhead, UK). Routinely, 4000 data points were collected during the first 5 s. Initial rates of DFP and $Fe^{3+}O$ species formation were determined from the linear fitting of the initial phases of the 650- and 350-nm traces (0.01–0.03 s). The reaction progress at high iron:protein ratio was followed after addition of 20 Fe^{2+} ions per subunit as the change of $A_{350\ nm}$ using rapid mixing (less than 10 ms) of 50 μM protein subunits (2.08 μM protein cages) in 200 mM MOPS, 200 mM NaCl, pH 7.0, with an equal volume of freshly prepared 1 mM ferrous sulfate in 1 mM HCl; the same UV/visible stopped-flow spectrophotometer was used, and 4000 data points were routinely collected in 1000 s [14]. Rates of $Fe^{3+}O$ mineralization were calculated from the linear fitting of the initial phases of the 350-nm traces.

2.4. $Fe^{3+}O$ mineral dissolution/chelation

Recombinant ferritin protein cages were mineralized with ferrous sulfate (20 Fe^{2+} ions per subunit) in 100 mM MOPS, 100 mM NaCl, pH 7.0 [14]. After mixing, the solutions were incubated for 2 h at room temperature and then overnight at 4 °C to complete the iron mineralization reaction. Fe^{2+} exit from caged ferritin minerals was initiated by reducing the ferritin mineral with added NADH (2.5 mM) and FMN (2.5 mM) and trapping the reduced and dissolved Fe^{2+} as the $[Fe(2,2'\text{-bipyridyl})_3]^{2+}$ complex outside the protein cage. Fe^{2+} release from the protein cage was measured as the absorbance of $[Fe(2,2'\text{-bipyridyl})_3]^{2+}$ at the maximum of $A_{522\ nm}$. The experiments were performed at two different iron and protein concentrations, 2.08 μM cages and 1.0 mM iron, and 1.04 μM cages and 0.5 mM iron respectively, with similar results. Initial rates were calculated using the molar extinction coefficient of $[Fe(2,2'\text{-bipyridyl})_3]^{2+}$ (8430 $M^{-1}\ cm^{-1}$) obtained from the slope of the linear plot (R^2 = 0.98–0.99) of the data related to the initial linear phase.

2.5. Sequence alignment

Sequence similarities with bullfrog M ferritin were analyzed to identify the nature of the amino acid present at positions corresponding to His54 using 500 sequences of vertebrate ferritins (identity range 100–55%) [16]. Search for ferritin from vertebrate sequences in

Please cite this article as: C. Bernacchioni, et al., Is His54 a gating residue for the ferritin ferroxidase site?, Biochim. Biophys. Acta (2015), http://dx.doi.org/10.1016/j.bbapap.2015.02.011

UniProtKB database was performed using BLAST and multiple sequence alignment was obtained by ClustalW.

2.6. Statistical analysis

The data were analyzed by Student's *t* test, and $P < 0.05$ was considered significant.

3. Results

The diferric-oxo-species and the ferric oxide $(Fe^{3+}O)_x$ that form at the second and third steps of the biomineralization reaction (see Introduction) are both characterized by an absorbance at 350 nm, although with different extinction coefficients; the short-lived DFP product of the first reaction steps has a characteristic absorbance at 650 nm. Stopped-flow electronic absorption kinetics allows monitoring the formation of these ferric species, after addition of iron(II) to apoferritin solutions [14,15,17]. Comparative kinetics data for the wild type and the H54A variant were used to monitor possible differences in the reaction efficiency using different Fe^{2+}/protein ratios.

Upon addition of 20 Fe^{2+}/subunit, i.e. with a stoichiometry that theoretically corresponds to 10 subsequent turnovers [14], we observed the behavior reported in Fig. 2A. The total amount of ferric-oxo species at plateau is the same for both wild type and H54A, but the initial rate is more than two times faster for the latter variant, as quantified in Fig. 2C, first column.

The biomineralization reaction is a complex phenomenon. After the catalytic oxidation of the ferrous species, under the effect of new incoming ferrous ions [8,18], the ferric products are released from the ferroxidase site and migrate towards the inner cavity, where they grow to provide a mineral of nanometer dimension [16]. NMR data have suggested that the migration process might involve ferric-oxo cluster of high nuclearity, but confirmatory high-resolution data are still missing [3,19]. Paramagnetic broadening of the NMR signals induced by ferric species formed in subsequent turnovers, has suggested that the path of ferric products from the catalytic site to the cavity involves the subunit area from the ferroxidase center to the short H5 helix, where also H54 is located [3,19]. To factorize out the possible contribution of His54 to Fe^{2+} entry into the ferroxidase site from its potential role in assisting ferric-product replacement with new ferrous ions, we have analyzed the kinetics at a lower number of turnovers. With 4 Fe^{2+}/subunit (Fig. 2B and C), the initial reaction rates of the DFP and ferric-oxo species formation in H54A ferritin variant, monitored at 650 nm and 350 nm respectively, are about 20% faster than the corresponding rates in wild type ferritin. In particular, at 650 nm the mean ± SD values of the initial rates obtained from three independent experiments are 1.75 ± 0.23 for the WT vs. 2.10 ± 0.19 for H54A; at 350 nm, 3.20 ± 0.50 for the WT vs. 3.93 ± 0.44 for H54A. Again, the total maximum absorbance does not change significantly for the two cage proteins. The situation is exactly the same when stopped-flow kinetics data are acquired with 2 Fe^{2+}/subunit (Fig. 2B and C), with the following mean ± SD values of the initial rates obtained from three independent experiments: at 650 nm, 0.50 ± 0.03 for the WT vs. 0.61 ± 0.08 for H54A; at 350 nm, 0.82 ± 0.14 for the WT vs. 1.02 ± 0.12 for H54A. Although the differences with respect to the wild type protein are statistically significant ($P < 0.05$), the effects with 4 and 2 Fe^{2+}/subunit are much attenuated compared to the stoichiometry of 20 Fe^{2+}/subunit. Consistently with the increased rate of formation of the ferric-oxo species, the decay of DFP is also faster in H54A than in wild type for both stoichiometries.

In summary, with low Fe^{2+}/subunit ratios, the observed speeding up of the reaction induced by the H54A mutation is meaningful but relatively weak (20% increase). Much stronger, instead, is the increase in initial rate of $(Fe^{3+}O)_x$ formation with 20 Fe^{2+}/subunit, suggesting a role for His54 in the release of ferric products from the catalytic site rather than in the uptake of ferrous ion from the inner cavity. Very importantly, for any stoichiometry the H54A substitution always results in an increased rate of product formation.

Exhaustive characterization of ferritin variants includes also the analysis of the caged biomineral dissolution induced by reducing and chelating agents [14,20–22]. In H54A the amount of iron released from the caged biomineral is unaffected by the mutation (Fig. 3). This result is not unexpected, as His54 is far from channels that have been proposed to control this process [14,20–22].

4. Discussion

Fe^{2+}-aqua ions enter the ferritin cage through the eight 3-fold symmetry channels that form where three subunits come in contact; the uptake of the metal ion is driven by an electrostatic gradient (or electric field gradient) generated by carboxylate protein residues located in the inner bottom part of these channels [8,9,14,23–25]. As proposed based on potential energy profile calculations and observed by X-ray crystallography, these residues can attract up to three Fe^{2+} ions into the inner bottom edge of the channels [8,12,25]. Once in, the inner cavity ferrous ions are imported into the catalytic reaction centers, located in the central inner part of the 4-helix bundle subunits. According to the X-ray data (PDB: 4LPJ, 4LQJ, 4LYX, 4LYU, 4LQV, 4LQN, 3RGD) [8,12], the permeability to iron of the ferroxidase site arises from a set of amino acids (E136, E57, H54) located in the close proximity of the catalytic center and facing the inner cavity of the cage. Substitution of conserved cage carboxylates E136 and/or E57 with Ala, slows down the catalytic reaction in bullfrog M ferritin, as recently demonstrated [11], supporting the idea that the translocation of cations from the inner cavity to the bundle interior is again driven by electrostatic attractions exerted by clusters of negatively charged residues.

Contrarily to what happens for E136A, E57A and E57AE136A, in H54A we observed a speeding up of the reaction, which becomes more evident at high turnover numbers. Obtaining an activation of an enzymatic reaction upon substitution of a natural amino acid with an Ala is quite a surprising result, whose interpretation is not obvious.

The presence of a residue potentially able to act as a metal ion ligand in positions structurally analogous to His54 of M ferritin is a common feature of catalytically active ferritin subunits.

In vertebrates H ferritins, the position corresponding to His54 is generally occupied by an Asn or a Gln (Q58 according the human H numbering) and in a few cases by a Tyr; those residues can play a role similar to His. Indeed, iron trapped at this site has been observed in crystal structures of the bullfrog M ferritin variant H54Q under iron free diffusion (PDB: 4ML5, 4MN9, 4MJY) [12]. An exception is represented by the ferritin from marine pennate diatom *Pesudonitzschia multiseries*, which is largely divergent from the other eukaryotic sequences [26], where the corresponding amino acid is an Asp, i.e. again a residue able to bind iron and other cations. The well-characterized archeal ferritin [18,27–29] from *Pyrococcus furiosus* also contains a Gln at this position.

In bacterioferritin from *Pseudomonas aeruginosa* a structurally similar position is occupied by His130, and the reorientation of its imidazole ring has been proposed to create a path for the translocation of iron from the ferroxidase center to the inner cavity [30]. This does not seem to be the case of His54 in bullfrog M ferritin, because in this hypothesis its substitution with a non-coordinating residue should lead to a decreased rate of biomineral formation, whereas we observed the opposite behavior (Fig. 2A).

Contrarily to the above cases, non-active subunits like the human L ferritin contain a Leu.

Paradoxically, in M ferritin the substitution of a coordinating hydrophilic residue by a hydrophobic non-coordinating one, like in non-active subunits, produces a variant that results to be an activator of the reaction. It should be noted, however, that in the fish *Gillichthys mirabilis* an Ala is naturally occurring in a ferritin subunit reported as active [31].

Please cite this article as: C. Bernacchioni, et al., Is His54 a gating residue for the ferritin ferroxidase site?, Biochim. Biophys. Acta (2015), http://dx.doi.org/10.1016/j.bbapap.2015.02.011

ARTICLE IN PRESS

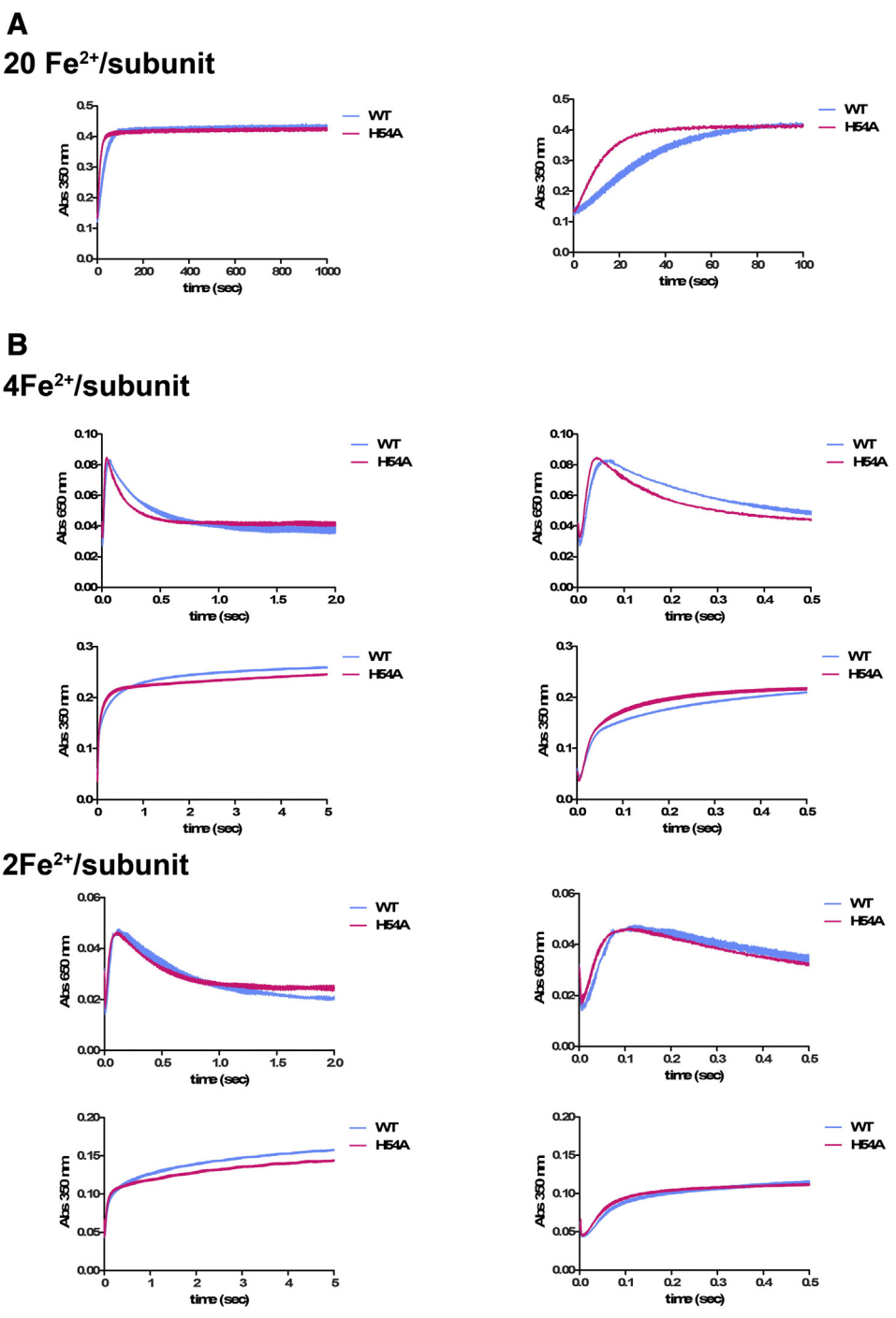

C

Initial rates of formation (fold-increase over WT values)

Protein	$(Fe^{3+}O)_x$ ($20Fe^{2+}$/subunit) ($\Delta A_{350\ nm}$/s)	DFP ($4Fe^{2+}$/subunit) ($\Delta A_{650\ nm}$/s)	$(Fe^{3+}O)_x$ ($4Fe^{2+}$/subunit) ($\Delta A_{350\ nm}$/s)	DFP ($2Fe^{2+}$/subunit) ($\Delta A_{650\ nm}$/s)	$(Fe^{3+}O)_x$ ($2Fe^{2+}$/subunit) ($\Delta A_{350\ nm}$/s)
H54A	2.4*	1.2*	1.2*	1.2*	1.2*

Fig. 2. Kinetics of products formation in WT and H54A by rapid-mixing, UV–vis spectroscopy. (A) Reaction progress at high iron:protein ratio (20 Fe^{2+}/subunit; 480 Fe^{2+}/cage) monitored as $(Fe^{3+}O)_x$ products ($A_{350\ nm}$) formation; the right panel shows an enlargement of the first 100 s. (B) Formation and decay of DFP intermediate ($A_{650\ nm}$) (left) and formation of $(Fe^{3+}O)_x$ products ($A_{350\ nm}$) (right) measured after the addition of 4 Fe^{2+}/subunit (upper panels) or 2 Fe^{2+}/subunit (lower panels); the right panels show enlargements of the first 0.5 s to highlight the differences in the initial rates. Each graph shows a set of curves (mean ± SEM) of a representative experiment of at least three. (C) Table reporting the fold change over WT (set as 1) of the initial rates of formation of the various species, calculated as described in Materials and methods section from three independent analyses. *Significantly different from the corresponding value in wild type; $P < 0.05$. WT: blue curves, H54A: pink curves.

Please cite this article as: C. Bernacchioni, et al., Is His54 a gating residue for the ferritin ferroxidase site?, Biochim. Biophys. Acta (2015), http://dx.doi.org/10.1016/j.bbapap.2015.02.011

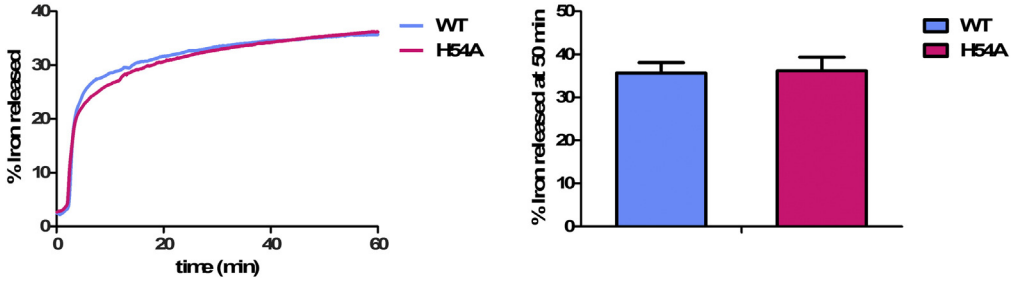

Fig. 3. Dissolution/chelation of iron from the ferritin biomineral formed in WT and H54A cages. Iron was recovered from caged hydrated ferric oxide mineral, synthesized by and inside ferritin protein cages, by adding reductant (NADH and FMN) in the presence of a chelator (2,2′-bipyridyl) and measuring the rate of formation of $[Fe(2,2'\text{-bipyridyl})_3]^{2+}$ outside the protein cage as described in Materials and methods section. One representative curve from three independent experiments is reported for both WT (blue) and H54A (pink) (left panel); the percentage of Fe^{2+} released at 60 min, calculated from three independent experiments performed with WT (blue) and H54A (pink), is shown in bar plot (right panel).

The present results highlight the importance of site directed mutagenesis and activity measurements to interpret correctly the results obtained via X-rays crystallography when unraveling the role of single amino acids in the mechanism of iron handling in the complex ferritin nanocages and their contribution to mechanistic variations among ferritins [32]. We showed that metal ions bound in wild type M ferritin crystals do not represent productive states for the ferritin reactions. From this study His54 seems to control the access of iron to the active site avoiding overloading, before the catalytic reaction has been completed and the ferric-oxy/hydroxo products have been released towards the inner cavity. His54 could also have a defense role by trapping non-natural divalent cations, thus keeping them far from the dinuclear iron site, where they compete with iron inhibiting the reaction [8,9]. It should be noted that the available structural data have been acquired under iron free diffusion and the largest effect on kinetics is again observed under excess iron in solution. The functional meaning of the present data for the *in vivo* function of ferritin is not clear at the present stage and would require in cell studies.

Transparency documents

The Transparency documents associated with this article can be found, in online version.

Acknowledgments

We acknowledge the financial support of MIUR PRIN 2012 (contract number 2012SK7ASN) and Ente Cassa di Risparmio di Firenze (contract number 2013.0494).

References

[1] E.C. Theil, R.K. Behera, T. Tosha, Ferritins for chemistry and for life, Coord. Chem. Rev. 257 (2013) 579–586.
[2] R.R. Crichton, J.P. Declercq, X-ray structures of ferritins and related proteins, Biochim. Biophys. Acta 1800 (2010) 706–718.
[3] D. Lalli, P. Turano, Solution and solid state NMR approaches to draw iron pathways in the ferritin nanocage, Acc. Chem. Res. 46 (2013) 2676–2685.
[4] F.M. Torti, S.V. Torti, Regulation of ferritin genes and protein, Blood 99 (2002) 3505–3516.
[5] P. Arosio, R. Ingrassia, P. Cavadini, Ferritins: a family of molecules for iron storage, antioxidation and more, Biochim. Biophys. Acta 1790 (2009) 589–599.
[6] J.K. Schwartz, X.S. Liu, T. Tosha, E.C. Theil, E.I. Solomon, Spectroscopic definition of the ferroxidase site in M ferritin: comparison of binuclear substrate vs cofactor active sites, J. Am. Chem. Soc. 130 (2008) 9441–9450.
[7] J. Hwang, C. Krebs, B.H. Huynh, D.E. Edmondson, E.C. Theil, J.E. Penner-Hahn, A short Fe–Fe distance in peroxodiferric ferritin: control of Fe substrate versus cofactor decay? Science 287 (2000) 122–125.
[8] I. Bertini, D. Lalli, S. Mangani, C. Pozzi, C. Rosa, E.C. Theil, P. Turano, Structural insights into the ferroxidase site of ferritins from higher eukaryotes, J. Am. Chem. Soc. 134 (2012) 6169–6176.
[9] T. Tosha, H.L. Ng, O. Bhattasali, T. Alber, E.C. Theil, Moving metal ions through ferritin-protein nanocages from three-fold pores to catalytic sites, J. Am. Chem. Soc. 132 (2010) 14562–14569.
[10] L. Toussaint, L. Bertrand, L. Hue, R.R. Crichton, J.P. Declercq, High-resolution structures of human apoferritin H-chain mutants correlated with their activity and metal-binding sites X-ray, J. Mol. Biol. 365 (2007) 440–452.
[11] R.K. Behera, E.C. Theil, Moving Fe^{2+} from ferritin ion channels to catalytic OH centers depends on conserved protein cage carboxylates, Proc. Natl. Acad. Sci. U. S. A. 111 (2014) 7925–7930.
[12] C. Pozzi, F. Di Pisa, D. Lalli, C. Rosa, E.C. Theil, P. Turano, S. Mangani, Time lapse, anomalous X-ray diffraction shows how Fe^{2+} substrate ions move through ferritin protein nanocages to oxidoreductase sites, Acta Crystallogr. D (2015) http://dx.doi.org/10.1107/S1399004715002333 (in press).
[13] M. Matzapetakis, P. Turano, E.C. Theil, I. Bertini, ^{13}C–^{13}C NOESY spectra of a 480 kDa protein: solution NMR of ferritin, J. Biomol. NMR 38 (2007) 237–242.
[14] E.C. Theil, P. Turano, V. Ghini, M. Allegrozzi, C. Bernacchioni, Coordinating subdomains of ferritin protein cages with catalysis and biomineralization viewed from the C4 cage axes, J. Biol. Inorg. Chem. 19 (2014) 615–622.
[15] T. Tosha, R.K. Behera, E.C. Theil, Ferritin ion channel disorder inhibits $Fe(II)/O_2$ reactivity at distant sites, Inorg. Chem. 51 (2012) 11406–11411.
[16] C. Bernacchioni, V. Ghini, C. Pozzi, F. Di Pisa, E.C. Theil, P. Turano, Loop electrostatics modulates the intersubunit interactions in ferritin, ACS Chem. Biol. 21 (2014) 2517–2525.
[17] X. Liu, E.C. Theil, Ferritin reactions: direct identification of the site for the diferric peroxide reaction intermediate, Proc. Natl. Acad. Sci. U. S. A. 101 (2004) 8557–8562.
[18] K.H. Ebrahimi, E. Bill, P.L. Hagedoorn, W.R. Hagen, The catalytic center of ferritin regulates iron storage via Fe(II)–Fe(III) displacement, Nat. Chem. Biol. 8 (2012) 941–948.
[19] P. Turano, D. Lalli, I.C. Felli, E.C. Theil, I. Bertini, NMR reveals pathway for ferric mineral precursors to the central cavity of ferritin, Proc. Natl. Acad. Sci. U. S. A. 107 (2010) 545–550.
[20] X. Liu, W. Jin, E.C. Theil, Opening protein pores with chaotropes enhances Fe reduction and chelation of Fe from the ferritin biomineral, Proc. Natl. Acad. Sci. U. S. A. 100 (2003) 3653–3658.
[21] W. Jin, H. Takagi, B. Pancorbo, E.C. Theil, "Opening" the ferritin pore for iron release by mutation of conserved amino acids at interhelix and loop sites, Biochemistry 40 (2001) 7525–7532.
[22] M.R. Hasan, T. Tosha, E.C. Theil, Ferritin contains less iron (^{59}Fe) in cells when the protein pores are unfolded by mutation, J. Biol. Chem. 283 (2008) 31394–31400.
[23] S. Levi, A. Luzzago, F. Franceschinelli, P. Santambrogio, G. Cesareni, P. Arosio, Mutational analysis of the channel and loop sequences of human ferritin H-chain, Biochem. J. 264 (1989) 381–388.
[24] A. Treffry, E.R. Bauminger, D. Hechel, N.W. Hodson, I. Nowik, S.J. Yewdall, P.M. Harrison, Defining the roles of the threefold channels in iron uptake, iron oxidation and iron-core formation in ferritin: a study aided by site-directed mutagenesis, Biochem. J. 296 (1993) 721–728.
[25] T. Takahashi, S. Kuyucaky, Functional properties of threefold and fourfold channels in ferritin deduced from electrostatic calculations, Biophys. J. 84 (2003) 2256–2263.
[26] A. Marchetti, M.S. Parker, L.P. Moccia, E.O. Lin, A.L. Arrieta, F. Ribalet, M.E. Murphy, M.T. Maldonado, E.V. Armbrust, Ferritin is used for iron storage in bloom-forming marine pennate diatoms, Nature 457 (2009) 467–470.
[27] K.H. Ebrahimi, E. Bill, P.L. Hagedoorn, W.R. Hagen, The catalytic center of ferritin regulates iron storage via Fe(II)–Fe(III) displacement, Nat. Chem. Biol. 8 (2012) 941–948.
[28] K.H. Ebrahimi, P.L. Hagedoorn, J.A. Jongejan, W.R. Hagen, Catalysis of iron core formation in *Pyrococcus furiosus* ferritin, J. Biol. Inorg. Chem. 14 (2009) 1265–1274.
[29] J. Tatur, W.R. Hagen, P.M. Matias, Crystal structure of the ferritin from the hyperthermophilic archaeal anaerobe *Pyrococcus furiosus*, J. Biol. Inorg. Chem. 12 (2007) 615–630.
[30] S.K. Weeratunga, S. Lovell, H. Yao, K.P. Battaile, C.J. Fischer, C.E. Gee, M. Rivera, Structural studies of bacterioferritin B from *Pseudomonas aeruginosa* suggest a gating mechanism for iron uptake via the ferroxidase center, Biochemistry 49 (2010) 1160–1175.
[31] A.Y. Gracey, J.V. Troll, G.N. Somero, Hypoxia-induced gene expression profiling in the euryoxic fish *Gillichthys mirabilis*, Proc. Natl. Acad. Sci. U. S. A. 98 (2001) 1993–1998.
[32] J.M. Bradley, G.R. Moore, N.E. Le Brun, Mechanisms of iron mineralization in ferritins: one size does not fit all, J. Biol. Inorg. Chem. 19 (2014) 775–785.